An Investigation of a Latent Heat Storage Porous Bed and Condensing Flow Through It

K. Vafai

M. Sözen

Department of Mechanical Engineering,
The Ohio State University,
Columbus, OH 43210

In this work the transient analysis of the behavior of a packed bed of encapsulated phase change material (PCM) and the condensing flow through it is presented. The rigorous model used assumes no local thermal equilibrium between the bed particles and the working fluid, and incorporates the inertia effects in the momentum transport by the use of the Ergun–Forchheimer equation. Condensation in the working fluid is investigated. Thermal charging of the packed bed is analyzed and compared for a sensible heat storage material as well as for different latent heat storage materials (PCMs).

1 Introduction

Packed bed heat storage units have been used extensively in a wide variety of applications. Packed beds as storage media are attractive, for they offer a compact structure due to their relatively greater heat storage capacity as compared to systems that utilize energy transporting fluid as the storage medium. Also due to the large surface area offered by packed beds for heat transfer between the energy transporting fluid and the bed particles, the process of energy transfer and storage becomes very efficient.

The earlier forms of packed bed energy storage units relied solely on the sensible heat capacity of solid bed particles for storing thermal energy. This form has been satisfactorily employed for various applications. However, certain applications may impose a limitation on the size and weight of the packed bed system utilized. For instance, in the case of a heat rejection system in pulsed space power supplies that incorporates packed beds, the reduction of mass and volume is of utmost importance. In such cases utilization of only the sensible heat capacity of a certain material for energy storage may not be efficient. The remedy to this can be found in the utilization of latent heat in the process of energy storage. Recently, encapsulated phase-change materials (PCM) have received considerable attention as energy storage materials. The use of an encapsulated PCM is very appealing since it makes the utilization of latent heat storage capacity possible. This is achieved by using a PCM that has a melting temperature within the temperature range of operation of the system incorporating the packed bed. The principal advantage of PCMs in packed beds is that the energy storage density of the bed is increased significantly and thus, the size and mass of the storage system required for a particular application are reduced proportionally.

Different PCMs have been considered for use in packed bed energy storage units in different applications. For applications over 450°C, significant consideration has been given to salts (Marianowski and Maru, 1977). Properties of different PCMs considered for storage of solar energy have been presented by Lane (1986). Ananthanarayanan et al. (1987) investigated the dynamic behavior of a packed bed utilizing encapsulated Al–Si shots, which have a melting temperature of 577°C. Air was used as the energy transporting fluid in their study. Pitts and Ji (1987) presented another study on transient thermal behavior of a latent heat storage packed bed, which utilized the inorganic compound hydrate PCM, $Na_2HPO_3 \cdot 12H_2O$. Torab and Chang (1988) investigated the use of encapsulated PCMs for thermal energy storage units in space power systems. They considered lithium hydride as the PCM and lithium as the transport fluid.

Different models have been developed for analyzing the transient behavior of latent heat storage packed beds. In the majority of these models, the superficial velocity of the working fluid is assumed to be constant. This fact reduces the system of governing equations to a set of energy equations for the working fluid and for the PCM, respectively. Although this is a satisfactory approach when the working fluid is incompressible, it is not so when the working fluid is a gas or vapor under high pressures. Moreover, when the working fluid itself undergoes phase change (condensation), a rigorous model, which consists of the governing energy mass, and momentum balance equations, in addition to the relevant coupling thermodynamic relations, has to be employed for a possible analysis of the phase-change and transport phenomena. In the present work we will undertake the analysis of such a problem with a rigorous model.

Transient behavior of a packed bed of spherical particles under the condensing flow conditions of the working fluid is studied in the present work. The range of temperatures considered in this study is 300–350 K. Refrigerant-12 (R-12, or dichloro-difluoro-methane) is chosen as the energy transport fluid for several reasons. First, it is a highly inert and stable compound and its critical temperature is above the range of temperatures considered in the present problem. Moreover, it has relatively high vapor density and capacitance compared with typical gases such as air. Different bed materials will be considered for the bed particles for qualitative comparison. These include two different encapsulated PCMs (myristic acid and lithium-nitrate-trihydrate) and one sensible heat storage material (1 percent carbon-steel).

The cases considered in the present work involve relatively high fluid velocities and therefore, the Ergun–Forchheimer relation is employed, rather than the Darcy equation, as the vapor phase momentum equation in order to account for the inertia effects. No local thermal equilibrium (LTE) is assumed to be present between the fluid and the solid (or PCM) phases, and the heat transfer between the working fluid and the bed particles is modeled by a convective heat transfer term.

In an earlier work the general characteristics of fluid flow and heat transfer through a porous bed were analyzed in depth (Vafai and Sözen, 1990); a systematic evaluation of the validity of the local thermal equilibrium and one-dimensional transport assumption was made and an assessment of the validity of each of these assumptions was presented in the form of error maps. In another study general characteristics of condensing

Contributed by the Heat Transfer Division for publication in the JOURNAL OF HEAT TRANSFER. Manuscript received by the Heat Transfer Division July 11, 1989; revision received January 30, 1990. Keywords: Packed and Fluidized Beds, Phase-Change Phenomena, Thermal Energy Storage.

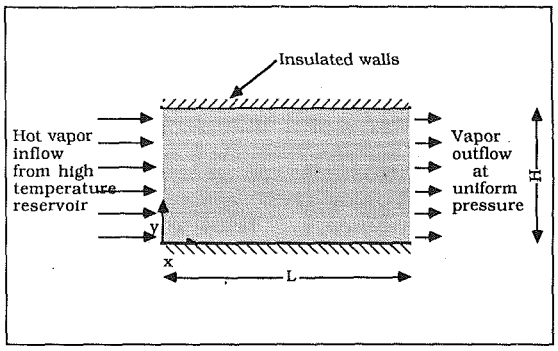

Fig. 1 Schematic diagram of the problem

flow through a porous bed were investigated (Sözen and Vafai, 1990) and it was shown that the pressure difference across the packed bed, the particle diameter, and the heat capacity of the solid phase have a profound effect on the condensation process in the packed bed.

The main objective of the present work is to analyze the thermal charging of a packed bed energy system for different forms of bed particle materials with emphasis on encapsulated phase change material. The time history of the crucial field variables such as the temperature profiles of the working fluid and the bed particles, and the velocity, density, and pressure of the working fluid will be determined. The determination of these quantities is important since the amount of energy flowing into and out of the packed bed, and hence the amount of energy stored in the packed bed as a function of time, can be determined from the time history of these variables.

2 Analysis

A general model has been developed for analyzing the phase change and transport phenomena in the thermal charging process of a packed bed. A schematic diagram of the problem considered in the present study is shown in Fig. 1. The packed bed, which is initially filled with R-12 at a slightly superheated state at uniform temperature and pressure, is subjected to a flow of superheated R-12 from a reservoir that has a higher temperature and pressure than those initially prevailing in the packed bed. Thus the problem becomes one with step change boundary conditions in temperature and pressure. The model developed for the analysis of the problem employs the following assumptions and simplifications:

1 The solid phase (or the PCM) and the liquid phase of the working fluid are incompressible.

2 The packed bed has uniform porosity and is isotropic.

3 Boundary and variable-porosity effects are neglected in the momentum equations.

4 Interparticle and intraparticle radiation heat transfer as well as thermal dispersion effects are neglected.

2.1 Governing Equations. It is customary to use the "local volume averaging" technique in order to develop a rigorous set of governing equations for the transport processes in porous media. It is necessary to make use of the two different averages of a quantity in the governing equations. These are the local volume average and the intrinsic phase average (Vafai and Sözen, 1990). While the local volume average of a quantity Θ associated with phase Ψ is defined as

$$\langle \Phi \rangle = \frac{1}{V} \int_{V_\Psi} \Phi dV \tag{1}$$

the intrinsic phase average of a quantity Φ associated with phase Ψ is defined as (Whitaker, 1977)

$$\langle \Phi \rangle^\Psi = \frac{1}{V} \int_{V_\Psi} \Phi dV \tag{2}$$

where V_Ψ represents the volume associated with phase Ψ. In using the volume averaging technique in the governing equa-

Nomenclature

$a_{\sigma\beta}$ = specific surface area common to σ and β phases, m^{-1}
$a_{\sigma\gamma}$ = specific surface area common to σ and γ phases, m^{-1}
A = constant in equation (11) = 23.485
B = constant in equation (11) = 2969.23, K^{-1}
c_p = specific heat at constant pressure, J kg^{-1} K^{-1}
d_p = particle diameter, m
Da = Darcy number = K/H^2
F = geometric factor defined in equation (13)
g = gravitational acceleration, m s^{-2}
G = mass velocity, kg m^{-2} s^{-1}
$h_{\sigma\beta}$ = fluid-to-particle heat transfer coefficient between σ and β phases, W m^{-2} K^{-1}
$h_{\sigma\gamma}$ = fluid-to-particle heat transfer coefficient between σ and γ phases, W m^{-2} K^{-1}
h_{sf} = specific latent heat of fusion, J kg^{-1}
H = height of the packed bed, m
k = thermal conductivity, W m^{-1} K^{-1}
$k_{r\beta}$ = relative permeability for fluid phase
$k_{\langle T \rangle}$ = coefficient of capillary pressure gradient with respect to temperature, N m^{-2}
k_ϵ = coefficient of capillary pressure gradient with respect to liquid volume fraction, N m^{-2}
K = permeability, m^2
L = length of the packed bed, m
$\dot{m}$ = condensation rate, kg m^{-3} s^{-1}
P = pressure, N m^{-2}
R_γ = gas constant for Refrigerant-12, J kg^{-1} K^{-1}
Re_p = particle Reynolds number = $\rho_\gamma v^* d_p/\mu_\gamma$
s = saturation = ϵ_β/ϵ
S = normalized saturation = $(s - s_{im})/(1 - s_{im})$
t = time, s
T = temperature, K
u = velocity component in x direction, m s^{-1}
v = velocity vector, m s^{-1}
ϵ = porosity
ϵ_β = volume fraction of liquid phase
ϵ_γ = volume fraction of vapor phase
ϵ_σ = volume fraction of solid phase
Δh_{vap} = latent heat of vaporization for Refrigerant-12, J kg^{-1}
Θ = dimensionless temperature = $(T - T_o)/(T_{in} - T_o)$
μ = absolute viscosity, kg m^{-1} s^{-1}
ρ = density, kg m^{-3}
$\rho_{\gamma,s}$ = saturation vapor density, kg m^{-3}

Subscripts

f = fluid (liquid + vapor)
feff = effective property for fluid
in = inlet
o = initial
β = liquid
γ = vapor
σ = solid
σeff = effective property for solid

Superscripts

f = fluid (liquid + vapor)
β = liquid
γ = vapor
σ = solid
$*$ = reference

Symbols

$\langle\,\rangle$ = "local volume average" of a quantity

tions, it is very important to distinguish between the properties that are associated with a single phase, such as the solid phase temperature, in which case one should use the intrinsic phase average, and the properties that have a characteristic average value over the averaging volume, such as the so-called "superficial fluid velocity," in which case one should use the spatial average or the local volume average value. These will help in presenting the exact and accurate form of the governing equations

With the assumptions and simplifications previously stated taken into account, the volume-averaged governing balance equations and the coupling relations are established as (Sözen and Vafai, 1990):

Vapor phase continuity equation

$$\frac{\partial}{\partial t}(\epsilon_\gamma \langle \rho_\gamma \rangle^\gamma) + \nabla \cdot (\langle \rho_\gamma \rangle^\gamma \langle \mathbf{v}_\gamma \rangle) = -\langle \dot{m} \rangle \tag{3}$$

Liquid phase continuity equation

$$\frac{\partial \epsilon_\beta}{\partial t} + \nabla \cdot \langle \mathbf{v}_\beta \rangle - \frac{\langle \dot{m} \rangle}{\rho_\beta} = 0 \tag{4}$$

Vapor phase equation of motion

$$\nabla \langle P_\gamma \rangle^\gamma = -\frac{\langle \rho_\gamma \rangle^\gamma F \epsilon_\gamma}{K_\gamma^{1/2}} [\langle \mathbf{v}_\gamma \rangle \cdot \langle \mathbf{v}_\gamma \rangle] \frac{\langle \mathbf{v}_\gamma \rangle}{|\langle \mathbf{v}_\gamma \rangle|} - \frac{\mu_\gamma}{K_\gamma} \langle \mathbf{v}_\gamma \rangle \tag{5}$$

which takes the following form with the second assumption cited above:

$$\frac{\partial}{\partial x} \langle P_\gamma \rangle^\gamma = -\frac{\langle \rho_\gamma \rangle^\gamma F \epsilon_\gamma}{K_\gamma^{1/2}} \langle u_\gamma \rangle^2 - \frac{\mu_\gamma}{K_\gamma} \langle u_\gamma \rangle \tag{5a}$$

Liquid phase equation of motion

$$\langle \mathbf{v}_\beta \rangle = -\frac{k_{r\beta} K}{\mu_\beta} \{ k_\epsilon \nabla \epsilon_\beta + k_{\langle T \rangle} \nabla \langle T_f \rangle^f + (\rho_\beta - \langle \rho_\gamma \rangle^\gamma) \mathbf{g} \} \tag{6}$$

Fluid phase energy equation

$$[\epsilon_\beta \rho_\beta (c_p)_\beta + \epsilon_\gamma \langle \rho_\gamma \rangle^\gamma (c_p)_\gamma] \frac{\partial \langle T_f \rangle^f}{\partial t} - \langle \dot{m} \rangle \Delta h_{\text{vap}}$$

$$+ [\rho_\beta (c_p)_\beta \langle \mathbf{v}_\beta \rangle + \langle \rho_\gamma \rangle^\gamma (c_p)_\gamma \langle \mathbf{v}_\gamma \rangle] \cdot \nabla \langle T_f \rangle^f = \nabla \cdot [k_{\text{feff}} \nabla \langle T_f \rangle^f]$$

$$+ h_{\sigma\beta} a_{\sigma\beta} [\langle T_\sigma \rangle^\sigma - \langle T_f \rangle^f] + h_{\sigma\gamma} a_{\sigma\gamma} [\langle T_\sigma \rangle^\sigma - \langle T_f \rangle^f] \tag{7}$$

Solid phase (PCM) energy equation

$$\epsilon_\sigma \rho_\sigma (c_p)_\sigma \frac{\partial \langle T_\sigma \rangle^\sigma}{\partial t} = \nabla \cdot [k_{\sigma\text{eff}} \nabla \langle T_\sigma \rangle^\sigma]$$

$$- h_{\sigma\beta} a_{\sigma\beta} [\langle T_\sigma \rangle^\sigma - \langle T_f \rangle^f] - h_{\sigma\gamma} a_{\sigma\gamma} [\langle T_\sigma \rangle^\sigma - \langle T_f \rangle^f] \tag{8}$$

Volume constraint relation

$$\epsilon_\sigma + \epsilon_\gamma(t) + \epsilon_\beta(t) = 1 \tag{9}$$

Equation of state for vapor phase

$$\langle P_\gamma \rangle^\gamma = \langle \rho_\gamma \rangle^\gamma R_\gamma \langle T_f \rangle^f \tag{10}$$

Thermodynamic relation for the saturation density of vapor

$$\rho_{\gamma,\, s} = \frac{\exp(A - B/T_f)}{R_\gamma T_f} \tag{11}$$

where A and B are known constants, T_f is in degrees Kelvin, and $\rho_{\gamma,\, s}$ is in kg/m^3. Equations (3)–(11) yield nine equations in nine unknowns, namely, $\epsilon_\beta(t)$, $\epsilon_\gamma(t)$, $\langle \rho_\gamma \rangle^\gamma$, $\langle \mathbf{v}_\gamma \rangle$, $\langle \mathbf{v}_\beta \rangle$, $\langle P_\gamma \rangle^\gamma$, $\langle T_f \rangle^f$, $\langle T_\sigma \rangle^\sigma$, and $\langle \dot{m} \rangle$.

The effective thermal conductivities of the working fluid and for the PCM (or solid phase) were modeled as

$$k_{\sigma\text{eff}} = \epsilon_\sigma k_\sigma$$

$$k_{\text{feff}} = \epsilon_\gamma k_\gamma + \epsilon_\beta k_\beta \tag{12}$$

The permeability for the vapor phase, K_γ, and the geometric factor, F, in the vapor phase momentum equation can be expressed as functions of ϵ_γ and d_p as given by Sözen and Vafai (1990). The relative permeability of the liquid phase is modeled in the form suggested by Udell and Fitch (1985) and given by Sözen and Vafai (1990).

Due to lack of better experimental findings, the value of immobile saturation, s_{im}, used by Kaviany and Mittal (1987), will be used in the present work. With the value of porosity taken to be equal to 0.39 as the average asymptotic value found by Benanati and Brosilow (1962) and s_{im} as 0.1, the critical value of the liquid fraction, $\epsilon_{\beta\text{crit}}$, below which the liquid phase is assumed to be immobile becomes 0.039.

Based on the specific surface area of a packed bed of spheres presented by Dullien (1979) as $a = 6(1-\epsilon)/d_p$, which was obtained from some geometric arguments, where ϵ is the porosity and d_p is the particle diameter, and also due to the fact that ϵ_β takes very small values (less than 0.01) in the problem considered, the specific surface area between the vapor phase and the bed particles can be accurately approximated as

$$a_{\sigma\gamma} = \frac{6(1-\epsilon_\gamma - \epsilon_\beta)}{d_p} \tag{13}$$

Also from an analysis of the representative length scales and volume scales of the liquid and vapor phases of the working fluid, one may obtain a relation between the specific surface areas $a_{\sigma\gamma}$ and $a_{\sigma\beta}$ as

$$a_{\sigma\beta} = a_{\sigma\gamma} \left(\frac{\epsilon_\beta}{\epsilon_\gamma} \right)^{2/3} \tag{14}$$

and hence

$$a_{\sigma\beta} = \frac{6(1-\epsilon_\gamma - \epsilon_\beta)}{d_p} \left(\frac{\epsilon_\beta}{\epsilon_\gamma} \right)^{2/3} \tag{15}$$

Empirical correlations found by Gamson et al. (1943) and originally expressed in the form of Colburn–Chilton j_h factors were found to be suitable for use in the present work. This decision was based on the fact that the particle size and particle Reynolds number ranges for these correlations covered the ranges considered in this work. Furthermore, the values of the void fraction and the fluid Prandtl number that were used in the experiments for establishing these correlations were very close to the respective values considered in the present investigation. After some manipulations these correlations can be expressed in the form given by Sözen and Vafai (1990) and repeated here for convenience:

$$h_{\sigma j} = 1.064 (c_p)_j G_j \left[\frac{c_p \mu}{k} \right]_j^{-2/3} \left[\frac{d_p G}{\mu} \right]_j^{-0.41}$$

$$\text{for } \frac{d_p G}{\mu} \geq 350 \qquad \text{(turbulent)}$$

$$h_{\sigma j} = 18.1 (c_p)_j G_j \left[\frac{c_p \mu}{k} \right]_j^{-2/3} \left[\frac{d_p G}{\mu} \right]_j^{-1} \tag{16}$$

$$\text{for } \frac{d_p G}{\mu} \leq 40 \qquad \text{(laminar)}$$

where G denotes the mass flux of phase j and j stands for β or γ for the liquid or the vapor phase, respectively.

It should be noted that due to the physical conditions of the problem, the liquid phase turned out to be essentially immobile. Therefore, $h_{\sigma\beta}$ practically assumes zero value and there is no need for $a_{\sigma\beta}$. However, for the sake of completeness of the model, these have been included in the model so that it becomes applicable to any condensation problem with funicular condensate.

2.2 Boundary and Initial Conditions. In the problem analyzed, the packed bed is initially filled with R-12 at uniform temperature and pressure and in local thermal equilibrium with the bed particles. Therefore, this condition is mathematically expressed as

$$T_f(x, y, t=0) = T_o$$
$$T_\sigma(x, y, t=0) = T_o \tag{17}$$
$$P_\gamma(x, y, t=0) = P_o$$

There is a continuous flow of high-temperature vapor into the packed bed from a reservoir while the pressure at the exit of the packed bed is maintained at the initial bed pressure. The following mathematical forms express these boundary conditions:

$$T_f(x=0, y, t) = T_{in}$$
$$P_\gamma(x=0, y, t) = P_{in} \tag{18}$$
$$P_\gamma(x=L, y, t) = P_{\text{out}} = P_o$$

where

$T_o = 300$ K, $P_o = 796$ kPa, $T_{in} = 350$ K, $P_{\text{out}} = 796$ kPa,

and $P_{in} = 811.2$ kPa

The top and bottom walls of the packed bed are insulated and so we have

$$\left.\frac{\partial T_\sigma}{\partial y}\right|_{y=0,\ y=H} = \left.\frac{\partial T_f}{\partial y}\right|_{y=0,\ y=H} = 0 \tag{19}$$

2.3 Solution. As may be seen from the model outlined in the previous section, the governing equations are strongly coupled and an analytical solution is not possible. Therefore numerical solution by a finite difference technique was employed. Explicit finite difference schemes were found to be more appropriate for solution of this problem. Forward Euler differencing was applied to temporal derivative terms, while central differencing was utilized in spatial derivative terms, except in the convective terms, in which upwind differencing was used instead of central differencing.

It should be noted that depending on whether phase change occurs in the working fluid or the PCM at a given location and instant in the packed bed, the governing equations and the solution format will take different forms. The details of the two-phase solution format algorithm are given in the work of Vafai and Whitaker (1986). It is assumed that condensation occurs when the density of the vapor becomes equal to the saturation vapor density.

When there is no phase change in either the working fluid or the bed particles, the field variables $\langle \rho_\gamma \rangle^\gamma$, ϵ_β, $\langle u_\gamma \rangle$, $\langle \mathbf{v}_\beta \rangle$, $\langle T_f \rangle^f$, $\langle T_\sigma \rangle^\sigma$, ϵ_γ, and $\langle P_\gamma \rangle^\gamma$ are determined from equations (3)–(10), respectively. At the same time $\rho_{\gamma,s}$ is determined from equation (11). This is done to determine when $\langle \rho_\gamma \rangle^\gamma$ determined by equation (3) with a zero $\langle \dot{m} \rangle$ terms exceeds $\rho_{\gamma,s}$. When this happens, $\langle \rho_\gamma \rangle^\gamma$ is replaced by $\rho_{\gamma,s}$ from equation (11), and equation (3) is then used for determining $\langle \dot{m} \rangle$.

On the other hand, the phase-change process in the PCM also needs special consideration. The following physical characteristics of the PCM are built into the solution algorithm. Once the PCM at a certain location and time reaches its melting temperature during the thermal charging of the packed bed, its temperature remains constant until phase change (melting) is complete in the capsules at that location. During this period, the solid phase (or PCM) energy equation should not be used for determining the solid phase (or PCM) temperature. However, the amount of heat that is transferred to the PCM while phase change occurs should be integrated in time in order to determine when the phase change is completed. Once phase change is completed in the PCM at a certain location, determination for the PCM temperature is switched back to solution from the PCM (or solid phase) energy equation with appropriate liquid PCM properties incorporated into the numerical scheme.

At each time step, after the PCM temperature reaches the melting temperature, the convective heat transfer rate from the working fluid to the PCM and conduction heat transfer rates to and from the PCM are all summed up (for node (i, j)) and taken into account. Furthermore, during a given time step both the net energy input to a unit volume of the PCM and the net total energy into the PCM up to the end of that time step were found. This process was carried on until the net total energy into the PCM becomes equal to the net latent heat energy encapsulated within the PCM.

The property values of the materials used in the numerical computations are $k_\gamma = 0.0097$ W/m K, $(c_p)_\gamma = 710$ J/kg K, $\mu_\gamma = 12.6 \times 10^{-6}$ kg/m s, $R_\gamma = 0.068759$ J/kg K, $\Delta h_{\text{vap}} = 111{,}300$ J/kg, $(c_p)_\beta = 1115$ J/kg K, $\mu_\beta = 179.2 \times 10^{-6}$ kg/m s, $\rho_\beta = 1190.35$ kg/m^3, $k_\beta = 0.0545$ W/m K.

For myristic acid (PCM1)

$c_p = 1590$ J/kg K, $k = 0.1$ W/m K,

$\rho = 860$ kg/m^3, for solid phase

$c_p = 2260$ J/kg K, $k = 0.1$ W/m K,

$\rho = 860$ kg/m^3 for liquid phase

For lithium-nitrate-trihydrate (PCM2)

$c_p = 2090$ J/kg K, $k = 0.5$ W/m K,

$\rho = 1550$ kg/m^3 for solid as well as liquid phase

For 1 percent carbon-steel

$c_p = 473$ J/kg K, $k = 43$ W/m K, $\rho = 7800$ kg/m^3

In the numerical runs L was chosen as 0.2 m and H as 0.1 m.

2.4 Stability and Accuracy of the Numerical Scheme. We employed a proper combination of Δt, Δx, and Δy in order to assure stability. This was done by a systematic decrease in the grid size until further refinement of the grid size or the Δt showed no more than 1 percent difference in the convergent results. The 41×21 grid configuration (which corresponds to a dimensionless Δx or Δy or 0.025) was found to yield sufficiently accurate solutions.

In order to gain confidence in the validity of the results of the computer program developed, we performed a benchmarking. Since there was no previous effort to solve the present problem with as rigorous a model as we have used, with as many field variables and governing equations, analytical solutions to simpler problems were considered. The benchmarking was carried out for the limiting cases with no phase change in either the working fluid or the PCM. The first check was performed for energy transport by a benchmark against the analytical solution of the Schumann model as presented by Riaz (1977). This was done by reducing the present model to the Schumann model by neglecting some terms in the energy equations. The second benchmark was related to momentum transport in an isothermal flow of an ideal gas through a porous medium. The analytical solution obtained by Kidder and La Habra (1957) by using perturbation methods was for a semi-infinite porous medium. But for small times, before any pressure propagation reaches the exit of the porous medium, the solution is applicable to finite length problems and hence to the present problem. Comparisons of the results from our program with these two analytical solutions are shown in an earlier work (Vafai and Sözen, 1990).

3 Results and Discussion

It is convenient to nondimensionalize some of the field variables in presenting the numerical solutions, and keep others in dimensional form to give a better understanding of the variations of the important parameter. The variables $\langle P_\gamma \rangle^\gamma$, $\langle \rho_\gamma \rangle^\gamma$, and $\langle u_\gamma \rangle$ are nondimensionalized with respect to the corresponding reference quantities P^*, ρ^*, and v^*. However, the pertinent parameters of the thermal charging of the packed bed and the condensation of the working fluid are presented in dimensional form for a unit width of the packed bed as a

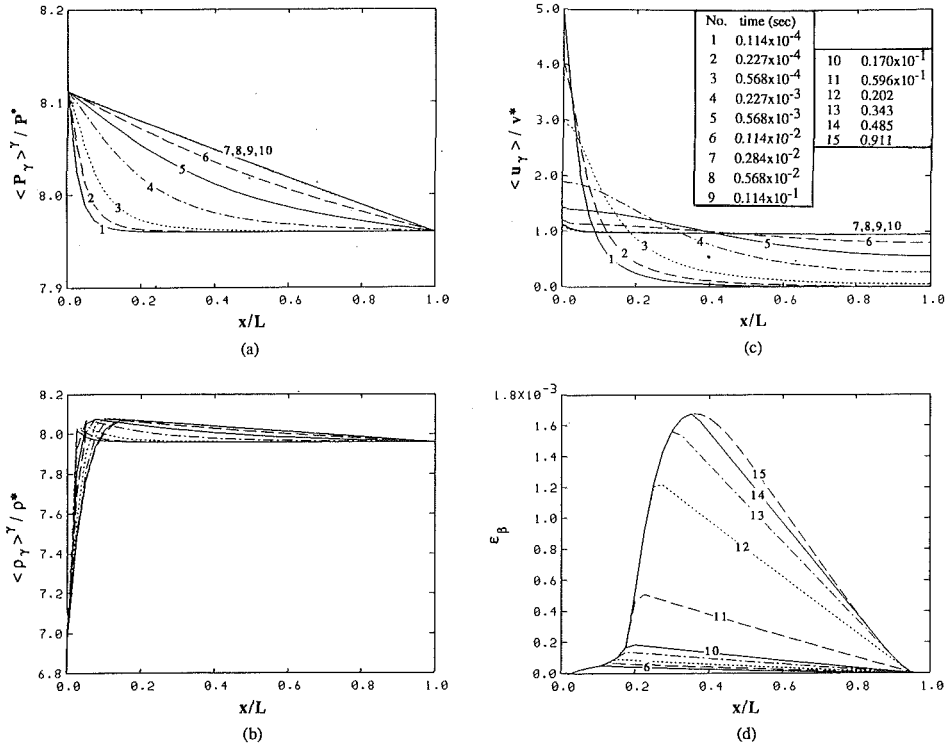

Fig. 2 Distribution of different field variables during the early stage

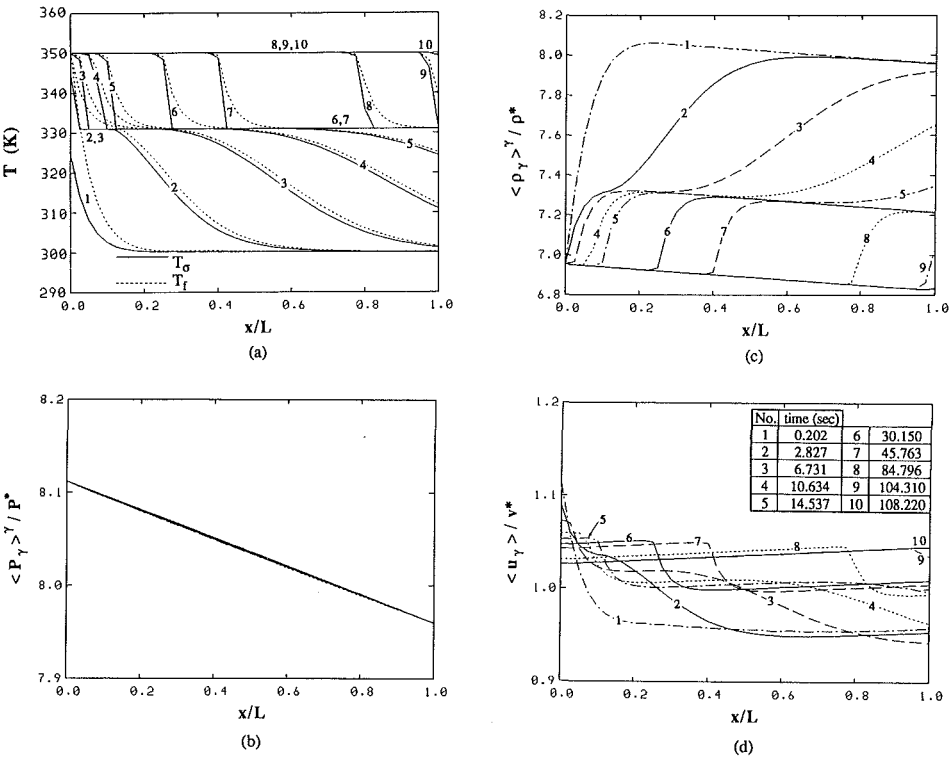

Fig. 3 Distribution of different field variables during the later stage

function of the dimensional time. The value chosen for P^* was 100 kPa, while ρ^* was then computed from the equation of state using P^* and the initial temperature T_o. The calculation of the reference velocity, v^*, was based on the vapor phase momentum equation by incorporating the global pressure difference applied across the packed bed and the vapor density as calculated from the equation of state by using the mean value of the inlet and exit pressures.

It should be noted that due to the nature of the problem it is not feasible to obtain totally generically applicable results for this problem. There are several main reasons for this. The first one is with respect to the condensation process. Since the density of the vapor is a function of temperature and pressure (by the equation of state) and the saturation vapor density is assumed to be a unique function of temperature, the condensation process is sensitive to the boundary and initial conditions

of the problem considered. For example, applying a given pressure difference across the packed bed at low operating pressure ranges, say around atmospheric pressure, will not result in any condensation, while applying the same magnitude of pressure difference at higher operating pressure ranges, say around 10 atm, will result in condensation. Therefore, although the pressure difference applied plays an important role in the condensation process, it is also important what ranges of operating pressures we are considering. For different vapors the condensation rate will be different for the same pressure difference applied since they have different heat of vaporization, different equations of state (i.e., gas constants), and different thermodynamic relations giving the saturation vapor density. Storage of energy in the packed bed cannot be scaled either, because thermal charging of the packed bed depends on the transient variation of the vapor exit temperature, which may be different for different PCMs. Also, due to the nature of the problem, the vapor mass flux into the packed bed is not uniform. Nevertheless, the results of this investigation will clearly show the generic qualitative features of transient condensing flow through a packed bed of encapsulated material.

It was found that in all the cases investigated in this study, the maximum local liquid fraction of the working fluid did not exceed the critical value above which the liquid becomes mobile, i.e., the liquid phase was always in a pendular state. This, combined with the fact that only insulated boundary conditions were considered in the present study, made the problem essentially one-dimensional. It was checked through numerical experimentation that the solution of the one-dimensional form of the governing equations did not have any appreciable difference from the solution to the two-dimensional form. Therefore, the two and one-dimensional solutions turned out to be the same. It should be emphasized that for insulated boundary conditions the lateral variations are not significant, and the only physical process that can make the problem two dimensional in this type of forced convective problem is the vertical motion of the liquid due to gravity. For such cases, however, much larger amounts of liquid that would make the liquid phase mobile have to be present.

Two distinct stages can be easily identified in the solution of the problem under consideration. First is an *early stage* with very strong transient effects, i.e., drastic spatial and temporal changes in the field variables, which lasts for a very short time. During the early stage the pressure distribution across the packed bed evolves and assumes an almost linear form, which is maintained afterward during the rest of the charging process, which will be referred to as the *later stage*.

The first PCM employed for the encapsulated bed particles is myristic acid, which has a melting temperature of 331 K. We will refer to this material as PCM1. The results for the case in which this material is used will be presented in detail. Once the high-pressure, high-temperature vapor is applied at the entrance of the packed bed, the vapor moving through the packed bed becomes compressed. Since it gives most of its excess internal energy to the colder PCM particles, its density reaches the saturation vapor density at certain locations and condensation takes place. Most of this condensation occurs in the early stage while the pressure distribution linearizes and the density of the vapor adjusts itself accordingly. Afterward, the vapor reaches superheated conditions at all locations and no more condensation takes place.

The early stage variations of the density, velocity, and pressure of the working fluid and the liquid fraction are shown in Fig. 2. The early stage is extended somewhat to include the period during which more than 99 percent of the condensation in the working fluid is completed. The consequence of the step change boundary condition can easily be seen from the high velocities at the inlet of the packed bed. These high velocities die out as the pressure distribution becomes linear. Except for a short thermal entry region, the changes in the field variables during the early stage are mostly pressure dependent because there is no appreciable thermal penetration. It should be noted that since the liquid fraction never reaches the critical value for becoming mobile, the ϵ_β distribution remains the same throughout the later stage.

The changes in the field variables during the later stage can be attributed to the development of the thermal penetration depth. As may be seen from Fig. 3, the pressure distribution remains linear. Variations of the temperatures of the working fluid and the PCM are very smooth until the PCM reaches its melting temperature. After the onset of melting in the PCM, a distinct discontinuity can be observed in the smoothness of the PCM temperature distribution. This is because for a certain length of the packed bed there is no change in the PCM temperature. In this region the working fluid also adjusts itself accordingly. This can be observed in the temperature profiles for time levels 2–8 in Fig. 3(*a*). This kind of qualitative behavior can also be seen in the vapor velocity and density variations along the packed bed at different time levels. For example, the vapor density variation is precisely and in a physically consistent manner related to pressure and temperature variations. It can also be noticed that there is an inverse relationship between vapor density and vapor velocity. This is due to the fact that the transient term in the vapor continuity equation loses its dominance and the convective term dominates during the later stage. Once the packed bed becomes thermally charged, then the vapor density distribution becomes linear, similar to the pressure distribution explained by the equation of state.

The variations of the average overall condensation rate and the cumulative condensate for a unit width of the packed bed are shown in Fig. 4. The overall condensation rate was computed by integrating the condensation rates at the individual grid points over the associated volumes. Integration of this over time yielded the accumulative condensate for a unit width of the packed bed. The effect of the variation of Δh_{vap} with temperature on condensation was also investigated. In Fig. 4 solid lines show the variations for constant value of Δh_{vap} of R-12, while dashed lines depict the variations for the case with Δh_{vap} varying as a function of temperature. The figure shows that there is a discrepancy of approximately 23 percent. The reason for this was that an average value for Δh_{vap} (for the temperature range of 300–350 K) was used in the results with constant Δh_{vap} value. The actual value of Δh_{vap}, however, drops from 137.78 kJ/kg to 98.35 kJ/kg as the temperature increases from 300 to 350 K. Since most of the condensation for this problem takes place in the early stage during which there is no appreciable thermal penetration in the packed bed, condensation takes place at temperatures close to the initial temperature, i.e., 300 K. Accordingly, the average value for Δh_{vap} for the 300–350 K range was too low and resulted in larger condensation. However, this practically did not have any appreciable effect on the thermal charging of the packed bed since the condensation process lasted only a very short time.

Of interest to the thermal charging of the packed bed are the rates of heat flowing into and out of the packed bed as a function of time. These were also computed for the given cross section of the packed bed for a unit width. The variations of these quantities are depicted in Fig. 5(*a*), except for a very short time section at the beginning of the charging process, which was left out to obtain a better scale on the figure. The variation of the net energy stored for a unit width of the packed bed as a function of time is also depicted in Fig. 5(*b*). At the beginning of the charging process, the vapor flowing out of the packed bed leaves at a low temperature close to the initial temperature, and thus there is a large difference between the heat flow rates at the inlet and at the exit. Hence the rate of energy storage is large. Afterward, for a major portion of the charging process, there is a uniform difference between the rates of heat flowing into and out of the packed bed causing a linear increase in the amount of energy stored. Once the

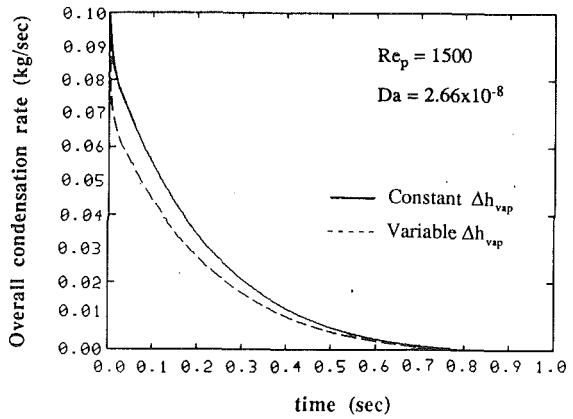

Fig. 4(*a*) Average overall condensation rate in the packed bed

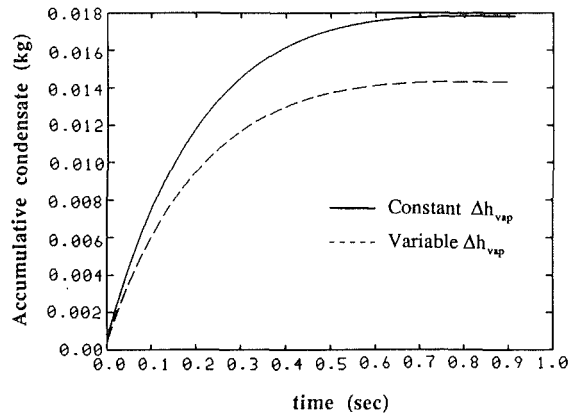

Fig. 4(*b*) Cumulative total condensate in the packed bed

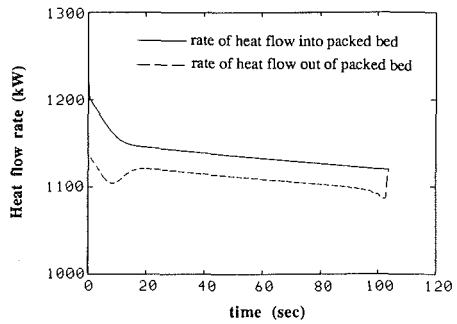

Fig. 5(*a*) Rates of heat flow into and out of the packed bed

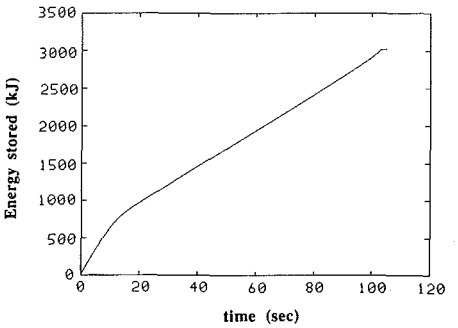

Fig. 5(*b*) Thermal charging of the packed bed

phase change is complete in all particles of the packed bed, both the working fluid temperature and the PCM temperature at the exit of the bed rise rapidly, causing a rapid decrease in the gap between the heat flow rates at the inlet and the exit.

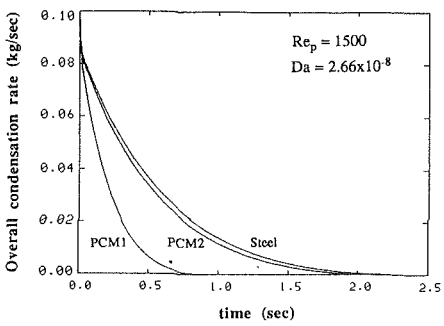

Fig. 6(*a*) Overall condensation rates in the packed bed for cases with different particle materials

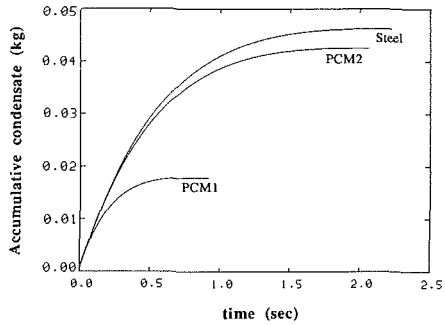

Fig. 6(*b*) Cumulative condensate in the packed bed for cases with different particle materials

3.1 *Qualitative Comparison of Condensation in the Working Fluid*. In addition to myristic acid (PCM1), two more materials were considered for the particles of the packed bed. These were lithium-nitrate-trihydrate, which we call PCM2, and 1 percent carbon-steel. Runs were made for these cases with the same initial and boundary conditions as in the case of PCM1. Figure 6 depicts the overall average condensation rate and condensate accumulation histories for all three cases. Since condensation in the working fluid takes place in a very short span of time at the beginning, with no significant thermal penetration in the packed bed, the difference in the results for the three materials considered can be attributed mainly to their physical properties. The capacitance of PCM2 differs only by 12 percent from that of steel, whereas that of PCM1 is almost three times smaller than that of steel. Due to this fact and the high heat transfer rate from the working fluid to the solid phase, the temperature propagation in both the solid phase and the working fluid is slower in the cases with steel and PCM2 than in the case with PCM1. Thus, for the former two cases it takes a longer time for condensation to stop. This is as a result of the longer time needed for the vapor to reach a high enough temperature for the vapor density to become lower than the saturation vapor density. Consequently, higher condensation rates are sustained for longer periods and larger condensate accumulations takes place in the case of steel and PCM2.

3.2 Qualitative Comparison of the Thermal Charging Process. The three materials considered for bed particles in this section are the same as those of the previous section. Time histories of the rates of heat flow into and out of the packed bed for the three cases are shown in Fig. 7, while that of the net energy stored in the packed bed for a unit width is shown in Fig. 8. It can be seen that, although at the beginning of the charging process the energy storage rate is almost the same for all three cases, it shows a different variation during later times. While that of the case with steel looks like a conventional

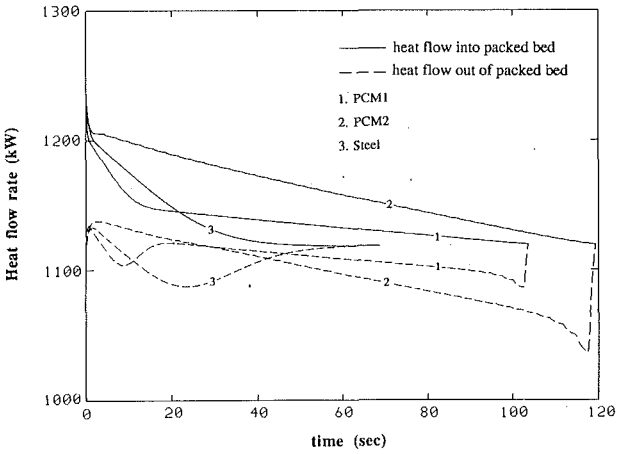

Fig. 7 Rates of heat flow into and out of the packed bed for cases with different particle materials

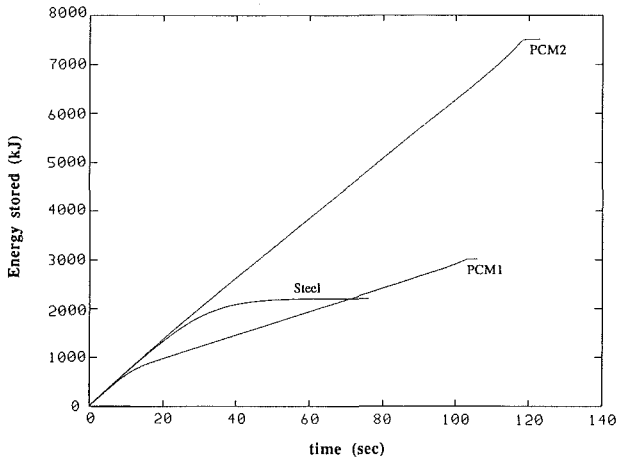

Fig. 8 Thermal charging of the packed bed for cases with different particle materials

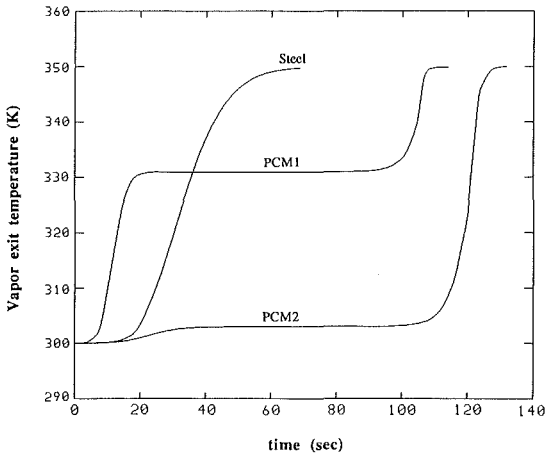

Fig. 9 Vapor exit temperature histories for cases with different particle materials

charging curve, which decays exponentially with time, the cases with the PCMs have a linear variation for a major portion of the charging period. These linear portions correspond to the time spans during which the temperature of the working fluid at the exit of the packed bed is fairly constant and approximately equal to the melting temperature of the PCM, since

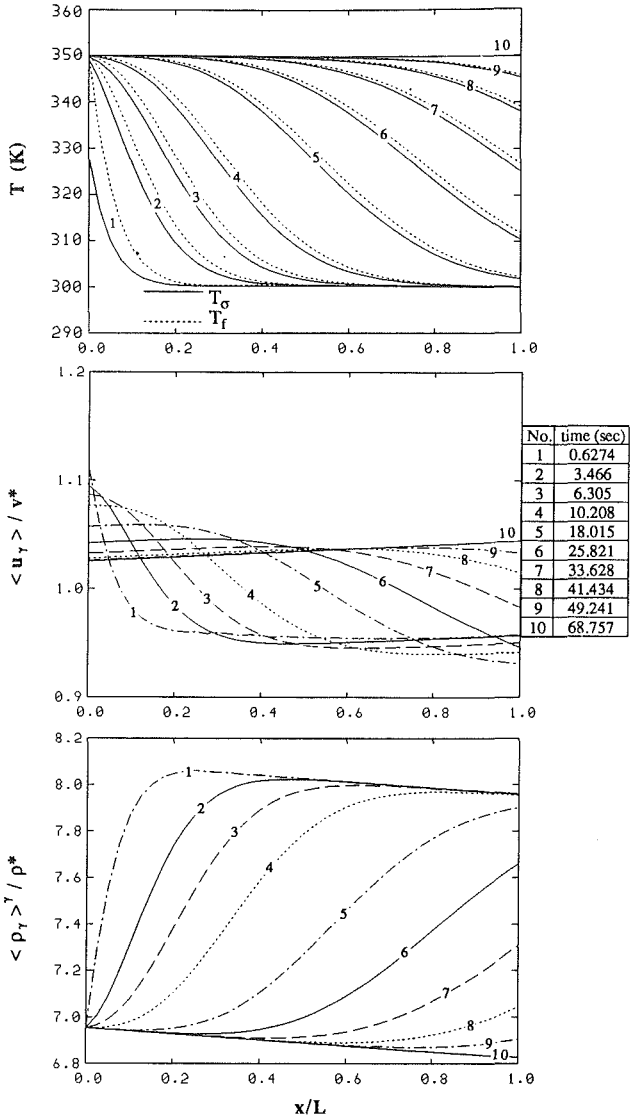

Fig. 10 Distribution of different field variables during the later stage for the case with steel bed particles

once the PCM reaches melting temperature its temperature remains constant until phase change is complete in the PCM. During this period the vapor temperature cannot drop below the melting temperature of the PCM and thus we have a fairly constant vapor exit temperature. In order to illustrate this more clearly, the time history of the vapor exit temperature is presented in Fig. 9 for the three cases.

Figure 8 also shows that using a PCM with a certain melting temperature may not always be a better choice over a sensible heat storage material. For instance, for the boundary conditions and the size considered in the present work, steel seems to perform better than PCM1 if we are interested in the energy storage range of up to 2200 kJ for a unit width. However, since PCM1 weighs significantly less than steel, the weight factor is also another important consideration entering these types of decision.

Figure 10 depicts the temperature profiles of the vapor and the solid phases and the variations of velocity and density of the vapor for the case with steel as the bed particle material. As can be seen, there are no sudden sharp changes in the temperature profiles of either the solid or the working fluid. Comparison of this figure with Fig. 2 explains the different behavior of the vapor exit temperature in the case of steel from those of the PCMs.

4 Conclusions

A rigorous model was developed for analyzing the transient behavior of a latent heat storage packed bed and the condensing flow through it. By this model it was possible to determine the time histories of all the field variables of interest. Qualitative comparisons of the transient behavior of a sensible heat storage and a latent heat storage packed bed have been presented. The difference between the two was very apparent in the thermal charging process. It was found that storage of thermal energy would be most efficient when a PCM with a melting temperature close to the lower limit of the operation temperature range is chosen. It was also found that for a given particle size and nominal particle Reynolds number, the amount of condensation in the working fluid depends principally on the thermophysical properties of the solid phase (or PCM), namely, the thermal capacitance of the packed bed; the larger the thermal capacitance of the bed the larger the amount of condensation in the working fluid. The results of this investigation clearly show the generic qualitative features of transient condensing flow through a porous bed made of encapsulated material.

Acknowledgments

A grant from the Ohio Supercomputer Center is gratefully acknowledged.

References

Ananthanarayanan, V., Sahai, Y., Mobley, C. E., and Rapp, R. A., 1987, "Modeling of Fixed Bed Heat Storage Units Utilizing Phase Change Materials," *Metallurgical Transactions B*, Vol. 18B, pp. 339–346.

Benanati, R. F., and Brosilow, C. B., 1962, "Void Fraction Distribution in Beds of Spheres," *AIChE Journal*, Vol. 8(3), pp. 359–361.

Dullien, F. A. L., 1979, *Porous Media Fluid Transport and Pore Structure*, Academic Press, New York.

Gamson, B. W., Thodos, G, and Hougen, O. A., 1943, "Heat, Mass and Momentum Transfer in the Flow of Gases Through Granular Solids," *Transactions AIChE*, Vol. 39, pp. 1–35.

Kaviany, M., and Mittal, 1987, "Funicular State in Drying of a Porous Slab," *Int. J. Heat Mass Transfer*, Vol. 30, pp. 1407–1418.

Kidder, R. E., and La Habra, 1957, "Unsteady Flow of Gas Through a Semi-infinite Porous Medium," ASME *Journal of Applied Mechanics*, Vol. 24, pp. 329–332.

Lane, G. A., 1986, *Solar Heat Storage: Latent Heat Material*, Vol. II, CRC Press, Inc., Boca Raton, FL.

Marianowski, L. G., and Maru, H. C., 1977, "Latent Heat Thermal Energy Storage Systems Above 450°C," presented at the 12th IECEC, Paper No. 779090, p. 555.

Pitts, D. R., and Ji, S., H., 1987, "Analysis of the Transient Thermal Performance of a Latent Heat Storage Packed Bed," in: *Multiphase Transport in Porous Media*, ASME FED-Vol. 60/HTD-Vol. 91, pp. 51–54.

Riaz, M., 1977, "Analytical Solution for Single- and Two-Phase Models of Packed-Bed Thermal Storage Systems," ASME JOURNAL OF HEAT TRANSFER, Vol. 99, pp. 489–492.

Sözen, M., and Vafai, K., 1990, "Analysis of the Non-thermal Equilibrium Condensing Flow of a Gas Through a Packed Bed," *Int. J. Heat Mass Transfer*, Vol. 33, pp. 1247–1261.

Torab, H., and Chang, W. S., 1988, "High Temperature Thermal Energy Storage for Power Systems," in: *Analysis of Time Dependent Thermal Systems*, ASME AES-Vol. 5, p. 71.

Udell, K. S., and Fitch, J., 1985, "Heat Transfer in Capillary Porous Media Considering Evaporation, Condensation and Non-condensible Gas Effects," in: *Heat Transfer in Porous Media and Particulate Flows*, ASME HTD-Vol. 46, pp. 103–110.

Vafai, K., and Sözen, M., 1990, "Analysis of Energy and Momentum Transport for Fluid Flow Through a Porous Bed," ASME JOURNAL OF HEAT TRANSFER, Vol. 112, pp. 690–699.

Vafai, K., and Whitaker, S., 1986, "Simultaneous Heat and Mass Transfer Accompanied by Phase Change in Porous Insulation," ASME JOURNAL OF HEAT TRANSFER, Vol. 108, pp. 132–140.

Whitaker, S., 1977, "Simultaneous Heat, Mass and Momentum Transfer in Porous Media: A Theory of Drying," *Adv. Heat Transfer*, Vol. 13, pp. 119–203.